RESEARCH ARTICLE

Fourier transform infrared spectroscopy study of ligand photodissociation and migration in inducible nitric oxide synthase [v1; ref status: awaiting peer review, http://f1000r.es/4ta]

Michael Horn[1], Karin Nienhaus[1], Gerd Ulrich Nienhaus[1,2]

[1]Karlsruhe Institute of Technology (KIT), Institute of Applied Physics, Karlsruhe, D-76131, Germany
[2]Department of Physics, University of Illinois at Urbana-Champaign, Urbana, IL, 61801, USA

v1 **First published:** 28 Nov 2014, **3**:290 (doi: 10.12688/f1000research.5836.1)
Latest published: 28 Nov 2014, **3**:290 (doi: 10.12688/f1000research.5836.1)

Abstract

Inducible nitric oxide synthase (iNOS) is a homodimeric heme enzyme that catalyzes the formation of nitric oxide (NO) from dioxygen and L-arginine (L-Arg) in a two-step process. The produced NO can either diffuse out of the heme pocket into the surroundings or it can rebind to the heme iron and inhibit enzyme action. Here we have employed Fourier transform infrared (FTIR) photolysis difference spectroscopy at cryogenic temperatures, using the carbon monoxide (CO) and NO stretching bands as local probes of the active site of iNOS. Characteristic changes were observed in the spectra of the heme-bound ligands upon binding of the cofactors. Unlike photolyzed CO, which becomes trapped in well-defined orientations, as indicated by sharp photoproduct bands, photoproduct bands of NO photodissociated from the ferric heme iron were not visible, indicating that NO does not reside in the protein interior in a well-defined location or orientation. This may be favorable for NO release from the enzyme during catalysis because it reduces self-inhibition. Moreover, we used temperature derivative spectroscopy (TDS) with FTIR monitoring to explore the dynamics of NO and carbon monoxide (CO) inside iNOS after photodissociation at cryogenic temperatures. Only a single kinetic photoproduct state was revealed, but no secondary docking sites as in hemoglobins. Interestingly, we observed that intense illumination of six-coordinate ferrous $iNOS_{oxy}$-NO ruptures the bond between the heme iron and the proximal thiolate to yield five-coordinate ferric $iNOS_{oxy}$-NO, demonstrating the strong trans effect of the heme-bound NO.

Open Peer Review

Referee Status: *AWAITING PEER REVIEW*

Discuss this article

Comments (0)

Corresponding author: Gerd Ulrich Nienhaus (uli@illinois.edu)

How to cite this article: Horn M, Nienhaus K and Nienhaus GU. **Fourier transform infrared spectroscopy study of ligand photodissociation and migration in inducible nitric oxide synthase [v1; ref status: awaiting peer review, http://f1000r.es/4ta]** *F1000Research* 2014, **3**:290 (doi: 10.12688/f1000research.5836.1)

Grant information: This work was supported by the Deutsche Forschungsgemeinschaft (Grant Ni291/10).
The funders had no role in study design, data collection and analysis, decision to publish, or preparation of the manuscript.

Competing interests: No competing interests were disclosed.

First published: 28 Nov 2014, **3**:290 (doi: 10.12688/f1000research.5836.1)

Introduction

Nitric oxide synthases (NOSs) are homodimeric heme enzymes that catalyze the oxidative degradation of L-arginine (L-Arg) to nitric oxide (NO)[1,2]. Three structurally similar NOS isoforms have been identified in endothelial cells (eNOS), neuronal tissues (nNOS) and in macrophages (iNOS)[3]. Different from eNOS and nNOS, iNOS is not expressed in resting cells but induced upon inflammatory and immunologic stimulation. Each NOS protomer consists of an oxygenase and a reductase domain. In the catalytic oxygenase domain (NOS_{oxy}), dioxygen (O_2) binds to a central heme prosthetic group, anchored to the polypeptide chain via a proximal cysteine residue (Figure 1). Its thiol sulfur atom accepts a hydrogen bond from an adjacent tryptophan residue. The substrate, L-Arg, is accommodated directly on top of the heme plane in the distal pocket; the cofactor tetrahydrobiopterin, H4B, binds along the side of the heme[4–7]. L-Arg and H4B are linked through an extended hydrogen bonding network mediated by one of the heme propionate groups. The reductase domain, NOS_{red}, binds flavin mononucleotide (FMN), flavin adenine dinucleotide (FAD), and reduced nicotinamide adenine dinucleotide phosphate (NADPH). It provides the electrons for the catalytic reaction proceeding in the oxygenase domain. In a first step, L-Arg is converted to N-hydroxy L-Arg (NOHA). Subsequently, NOHA is decomposed into citrulline and nitric oxide (NO). Electron transfer is enabled by calmodulin binding in the interface between the two domains[8].

The NO molecule generated during enzymatic turnover can either coordinate directly to the heme iron or diffuse out of the protein into the environment. From there, it may again bind in a bimolecular process[9]. Formation of the very stable ferrous NO complex results in self-inhibition of the enzyme. The probability of forming this product depends on the dissociation rate coefficient of NO from the ferric heme, the likelihood of autoreduction of the ferric NO-bound form to the ferrous derivative with its much stronger NO affinity, and the probability of oxidizing the ferrous NO-bound species to the ferric form plus nitrate by O_2[10]. Deactivation of the enzyme may also occur via nitrosylation of the side chains of two cysteine residues coordinating a zinc ion in the dimer interface, which leads to irreversible dissociation into non-functional monomers[11–14].

The iNOS isoform has been implicated in the pathogenesis of various diseases; so there is a growing interest in developing potent and highly selective inhibitors[15,16]. Their targeted design requires detailed insights into the interactions between ligand, substrate and the surrounding protein matrix. Therefore, we have investigated ligand and substrate binding in the iNOS oxygenase domain, $iNOS_{oxy}$, by using Fourier transform infrared (FTIR) spectroscopy of the stretching vibrations of carbon monoxide (CO) and NO as ligands rather than the physiological ligand O_2. They are of similar size as O_2, which suggests that ligand dynamics within the protein may be comparable for all three ligands. CO and NO both have excellent properties as infrared (IR) spectroscopic probes[17]. CO has proven to be an attractive heme ligand because the CO bond stretching vibration gives rise to strong mid-IR absorption bands that can be measured with exquisite sensitivity and precision[17,18]. The IR bands are fine-tuned by electrostatic interactions with the environment[19–21]; therefore, CO is frequently utilized as a local probe of protein structure and dynamics[22].

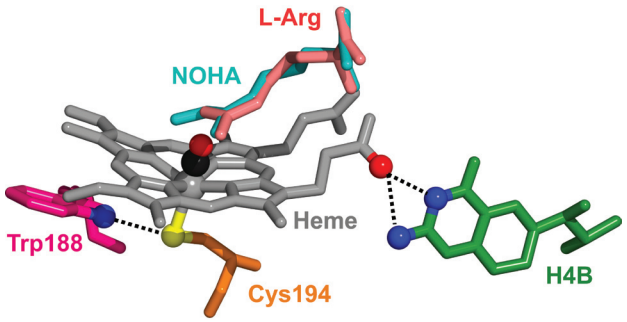

Figure 1. Schematic depiction of the $iNOS_{oxy}$ active site (pdb codes 1NOD and 1DWV). The CO ligand was added for illustration.

In the gas phase, CO absorbs at 2143 cm^{-1} [23]. When bound to the central iron of a heme cofactor, the CO stretching frequency, ν_{CO}, which is typically in the 1900 – 2000 cm^{-1} spectral range, is susceptible to changes in the iron-ligand bond and the local electric field due to the vibrational Stark effect[24–29]. There are two major contributions to the heme iron-CO bond, *i.e.*, σ-donation from a weakly antibonding 5σ MO of CO to the iron 4s and $3d_z^2$ orbitals and π-backbonding from the iron $3d_z$ orbitals to the strongly antibonding CO 2π* orbital[30]. A positive charge located near the CO oxygen attracts electron density, causing a decrease in σ-donation and an increase in backbonding. Consequently, the C–O bond order is reduced and ν_{CO} shifts to lower values[19–21]. A negative charge has the opposite effect.

After photodissociation of CO-bound heme protein samples, the stretching bands of unbound CO trapped inside a protein are found within the range from ~2080 to ~2160 cm^{-1} [18,31]. The vibrational bands can reveal changes related to ligand relocation to other sites within the protein[18,29,32,33], rotational motions of the ligand in these sites[25,34] and protein conformational changes[35]. Often, there are doublets of bands corresponding to opposite orientations of the CO at a particular transient docking site[27,29,32,36–38]. The bond order and, therefore, ν_{CO} increases if the carbon atom interacts with a hydrogen bond donor, whereas an interaction with the ligand oxygen reduces both the bond strength and the stretching frequency[29].

Unlike CO, which only binds to a ferrous (Fe^{II}) heme iron, NO may coordinate to both the ferrous and the ferric (Fe^{III}) forms. So far, FTIR studies using NO have remained scarce because of its weaker intrinsic absorption. Furthermore, there is spectral overlap with the amide bands and ultrafast recombination of a major fraction of proteins even at very low temperatures. Therefore, only small photoproduct yields are obtained in experiments probing longer times such as FTIR, which renders experiments with ferrous NO technically challenging. Consequently, we have limited ourselves to NO binding to ferric heme in this work. For iNOS, this complex is of physiological relevance because the heme iron is in the ferric state after completion of the catalytic cycle.

Here, we have performed FTIR studies on iNOS at cryogenic temperatures, at which ligand rebinding is very slow. Thus, photoproducts induced by illumination are long-lived and can be conveniently

studied by photolysis difference spectroscopy. Moreover, essentially all protein (and solvent) motions are frozen in[39,40], so the ligands cannot escape to the solvent and can be observed within the protein matrix. We have combined FTIR with temperature-derivative spectroscopy (TDS)[41–43], which allows us to disentangle photolysis-induced absorption changes caused by the different types of ligand dynamics.

Materials and methods

Protein expression

The $iNOS_{oxy}$ domain, with its first 65 residues deleted ($\Delta65$ $iNOS_{oxy}$, referred to as $iNOS_{oxy}$ in the following), was expressed essentially as described[44]. Briefly, $iNOS_{oxy}$ containing plasmids (pCWori) were transformed into competent *Escherichia coli* cells (strain BL21). The cells were plated on agar in the presence of 390 µM ampicillin (Carl Roth, Karlsruhe, Germany) and cultured overnight at 37°C. A single colony was added to 150 ml terrific broth (TB, Carl Roth) supplemented with ampicillin (390 µM) and agitated for 12 h at 37°C and 250 rpm. 10 ml of the overnight culture were added to 1.5 l TB, containing 390 µM ampicillin, and grown to an optical density of ~1 at 600 nm. Then, the temperature was lowered to 30°C and δ-aminolevulinic acid (44 µM, Sigma-Aldrich, St. Louis, MO, USA) and hemin (8 µM, Sigma-Aldrich) were added. iNOS expression was induced by adding isopropyl β-D-1-thiogalactopyranoside (IPTG, Carl Roth) to a final concentration of 100 µM. After 48 h (fresh ampicillin was added every 16 h), the cells were harvested by centrifugation for 20 min at 4°C and 2,000 rpm (swing-bucket rotor, 4–16 K, Sigma, Osterode, Germany). The cells were resuspended in lysis buffer (40 mM HEPES, 10% glycerol (vol.), 200 mM NaCl, pH 7.6, Carl Roth), mixed with 2 mg DNase (Sigma-Aldrich), and ruptured using a bead-beater (Biospec, Bartlesville, USA), filled with 0.1 mm (diameter) zirconia/silica beads (three treatments of 2 min each). The lysate was separated from the beads by a glass filter and loaded onto an immobilized-metal ion affinity column equilibrated with lysis buffer (Ni Sepharose 6 FastFlow, GE Healthcare). After washing with lysis buffer supplemented with increasing concentrations of imidazole (0, 10, 40 mM, Sigma-Aldrich), the protein was eluted with lysis buffer containing 160 mM imidazole. Appropriate fractions were pooled, dialyzed against water and concentrated by using Vivaspin Turbo 15 (cut-off 10 kDa) centrifugal concentrators (Sartorius, Göttingen, Germany). Finally, the protein was lyophilized and stored at -20°C.

Sample preparation

To prepare CO-ligated $iNOS_{oxy}$, 12 mg freeze-dried iNOS were slowly added to 40 µl cryosolvent (75%/25% glycerol/100 mM potassium phosphate buffer (v/v), pH 7.4, and, if so desired, supplemented with L-Arg and NOHA substrate (Sigma-Aldrich) or H4B cofactor (Sigma-Aldrich) to reach final concentrations of 200 mM and 100 mM, respectively) and stirred under 1 atm CO for 60 min. Subsequently, a two-fold molar excess of an anaerobically prepared sodium dithionite solution (Sigma-Aldrich) was added with a gas-tight Hamilton syringe, and the solution was stirred for another 10 min. To remove any undissolved protein, the solution was centrifuged for 10 min at 13,400 rpm (Minispin centrifuge, Eppendorf, Hamburg, Germany) before loading it into the sample cell. For an NO-ligated sample, ferric $iNOS_{oxy}$ was dissolved in cryosolvent and stirred under an N_2 atmosphere for 1 h. The gas phase above the sample was replaced repeatedly by N_2 to efficiently remove O_2. Finally, a few microliters of NO gas were added with a gas-tight syringe. NO ligation to the heme iron was confirmed by UV/vis absorption spectroscopy.

Experimental setup

A few microliters of the sample solution were sandwiched between two CaF_2 windows (diameter 25.4 mm) separated by a Mylar washer. The windows were mounted inside a block of oxygen-free high-conductivity copper. The copper block was attached to the cold-finger of a closed-cycle helium refrigerator (model F-50, Sumitomo, Tokyo, Japan). The sample temperature was measured with a silicon temperature sensor diode and regulated in the range 3 – 320 K by a digital temperature controller (model 336, Lake Shore Cryotronics, Westerville, OH). A continuous-wave, frequency-doubled Nd-YAG laser (Samba, Cobolt, Solna, Sweden), emitting up to 300 mW output power at 532 nm, was used to photolyze the sample. The laser beam was split and focused with lenses on the sample from both sides. Transmission spectra were recorded on a Vertex 80v FTIR spectrometer (Bruker, Karlsruhe, Germany) at a resolution of 2 cm^{-1}, using either an InSb detector (75 µm thick Mylar, 1,700 to 2,300 cm^{-1}) or an MCT detector (<5 µm thick Mylar, 1,100 to 2,300 cm^{-1}).

FTIR photolysis difference spectroscopy

The infrared absorption of CO and NO can be studied selectively by using photolysis difference spectroscopy, which involves measurement of IR transmission spectra, $I(\nu, T)$, before and after photolysis. The difference absorbance of the two spectra, $\Delta A(\nu, T) = \log(I_{dark}/I_{light})$, contains only features that are due to photodissociation of the ligand from the heme iron. The missing absorption of the heme-bound ligands (A bands) after photolysis and the corresponding absorption of the photolyzed ligands (photoproduct bands) are displayed with negative and positive amplitudes, respectively. Peak positions and fractional occupancies were determined by fits with Gaussian band shapes; they are compiled in Table 1. In the following, we use the Gaussian band positions (frequencies) at 4 K as a subscript to 'A' (denoting the heme-bound state) to distinguish the absorbance bands and also to refer to a particular substate of the protein.

Different illumination protocols were applied for photodissociation[17]. Before starting a TDS experiment, the sample was illuminated for 10 s at 4 K to trap the photolyzed ligand close to the heme iron at the so-called primary docking site B. Alternatively, under 'slow-cool' illumination, the sample was cooled from 160 to 4 K at a rate 0.3 K/min under constant laser illumination to enable the photodissociated ligands to sample alternative docking sites that may not be accessible upon photolysis at 4 K. In both protocols, 300 mW laser power at 532 nm was used. To monitor the photodissociation kinetics, the samples were continuously illuminated for 15,000 s at reduced laser power (0.3 mW or 10 mW), and transmission spectra were recorded continuously. For comparison, the photolysis yield was scaled with respect to complete photodissociation with full laser power (300 mW).

Temperature derivative spectroscopy (TDS)

TDS, an experimental protocol designed to study thermally activated rate processes involving enthalpy barrier distributions, has been

Table 1. Positions and fractional areas of the IR stretching bands of heme-bound and photodissociated CO and NO ligands in $iNOS_{oxy}$ samples, determined at 4 K with estimated experimental errors of ± 0.5 cm^{-1} and ± 3%, respectively.

	Heme-bound CO		Photolyzed CO (10 s @ 4 K)		Photolyzed CO (Slow cool)		Heme-bound NO		NO Photoproduct	
	cm^{-1}	%	cm^{-1}	%	cm^{-1}	%	cm^{-1}	%	cm^{-1}	%
w/o substrate	1921	9	2124	55	2124	85	1870	100	1814	23
	1945	40	2129	45	2132	15			1818	77
	1959	51								
L-Arg	1904	69	2120	28	2120	20	1829	56	1814	13
	1921	13	2131	28	2131	34	1847	16	1822	87
	1951	18	2144	32	2145	30	1870	28		
			2150	12	2150	16				
NOHA	1903	13	2122	75	2117	20	1851	15	1814	30
	1937	57	2133	19	2124	44	1870	85	1818	70
	1956	30	2145	6	2133	36				
H4B	1924	18	2124	75	2122	10	1872	82		
	1951	82	2133	25	2126	61	1890	18		
					2134	29				

described in great detail elsewhere[41–43]. Briefly, a non-equilibrium state is created in the sample at low temperature, *e.g.*, by photolysis with visible light. The integrated absorbance, *A*, of a spectral band taken at the lowest temperature represents the total photolyzed population, *N*. Subsequently, thermal relaxation of the sample back to equilibrium is recorded while the sample temperature is ramped up linearly over a few hours in the dark. One FTIR transmission spectrum is taken for every 1-K temperature increase. In the simplest analysis, we assume that any change in integrated absorbance is due to ligand rebinding and, therefore, proportional to a population change, ΔN, during acquisition of two successive spectra. TDS data are conveniently presented as two-dimensional contour plots, with solid lines indicating an absorbance increase and dashed lines a decrease. Contours are spaced logarithmically to emphasize small features.

Results and discussion

1. FTIR spectroscopy of $iNOS_{oxy}$ using CO as an internal probe

In the following, we present 4-K FTIR photolysis difference spectra of $iNOS_{oxy}$-CO and briefly discuss the influence of substrate, substrate intermediate and cofactor on the CO stretching vibration and rebinding. For additional information, we refer to Jung *et al.*[45] and Li *et al.*[46].

Photolysis difference spectra at 4 K. The 4-K absorption difference spectrum of $iNOS_{oxy}$-CO displays two broad, extensively overlapping A bands at 1945 and 1959 cm^{-1}, indicative of two active site subconformations with significant intrinsic structural heterogeneity (Figure 2a). Adding the H4B cofactor induces only small changes; the resulting spectrum can be described by a dominant A band centered on 1951 cm^{-1} and a minor one at 1924 cm^{-1} (Figure 2a). As H4B binds along the side of the heme[4] and, thus, not in the immediate vicinity of the heme-bound CO, it is not expected to modify ν_{CO} to any significant extent. In contrast, the presence of L-Arg shifts the main A band of $iNOS_{oxy}$-CO/L-Arg to 1904 cm^{-1}; smaller features are located at 1921 and 1951 cm^{-1} (Figure 2a). The pronounced red-shift of A_{1904} arises from the electron-withdrawing effect of the terminal, positively charged NH_2^+ moiety of the L-Arg side chain close to the bound CO[4]. The position of the A_{1921} band is indicative of an electrostatic interaction of the CO dipole with a less pronounced positive partial charge, most likely the neutral terminal amino group of the L-Arg side chain.

If the reaction intermediate NOHA is present, three A bands at 1903, 1937 and 1956 cm^{-1} are discernable (Figure 2a). The crystal structure shows that NOHA binds in the same orientation in the active site as L-Arg, with the side chain pointing towards the heme iron[47]. Therefore, we suggest that, in those $iNOS_{oxy}$ molecules absorbing within the A_{1937} band, a hydrogen bonding interaction exists between the CO ligand and the hydroxyl group of the NOHA side chain. A_{1903} is most likely associated with $iNOS_{oxy}$ molecules, in which the terminal amine of the NOHA side chain is protonated (pK = 8.1[48]) and points towards the heme-bound CO. The protonated NOHA has been suggested to be the catalytically active substrate intermediate[49,50].

The absorption spectra of photolyzed CO are plotted in Figures 2b (brief illumination at 4 K) and 2c (slow-cool illumination); peak positions and relative areas are included in Table 1. For comparison, the integrated absorption in each spectral region was scaled to the same area. We note that the ratio of the integrated areas of the A and photoproduct bands is ~20[18].

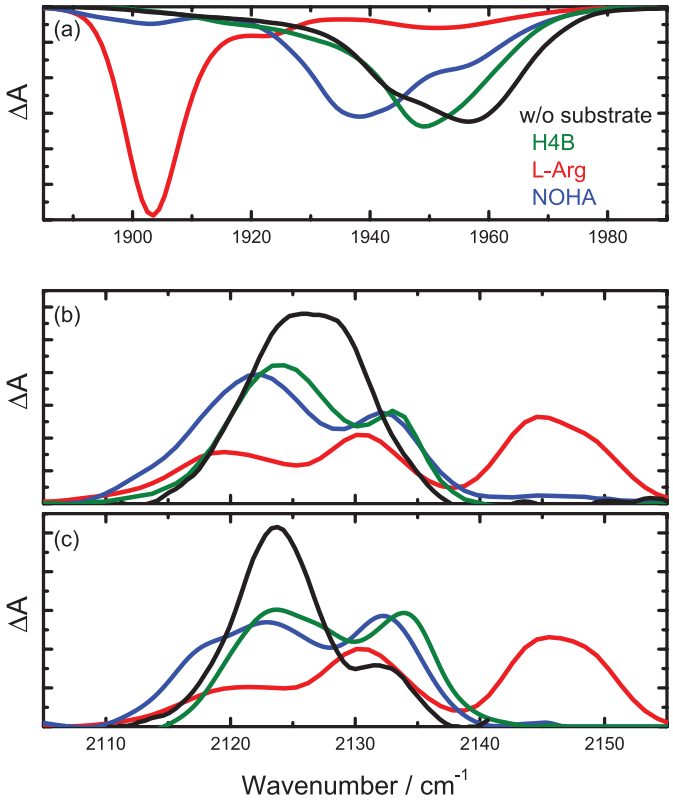

Figure 2. 4-K photolysis difference spectra of iNOS$_{oxy}$-CO. (**a**) Absorption of the heme-bound CO. (**b**) Photoproduct bands obtained after 10-s illumination at 4 K. (**c**) Photoproduct bands obtained after constant illumination during slow cooling from 160 to 4 K.

All photoproduct spectra obtained after 10-s illumination at 4 K have absorption bands in the 2120 – 2130 cm^{-1} spectral range (Figure 2b). The spectrum of iNOS$_{oxy}$-CO is composed of two stretching bands at 2124 and 2129 cm^{-1}. With H4B, photoproduct bands appear at 2124 and 2133 cm^{-1}, indicating that the cofactor has an effect on ν_{CO} of the unbound CO. In the presence of L-Arg, the absorption bands are centered on 2120 and 2131 cm^{-1}, and there are two additional bands at 2144 and 2150 cm^{-1}. Their higher stretching frequencies suggest formation of a hydrogen bond between the ligand carbon and the terminal amine group of L-Arg[29]. Upon NOHA binding, the photoproduct bands are centered on 2122 and 2133 cm^{-1}. The minor absorption at 2145 cm^{-1} can be associated with CO ligands photolyzed from iNOS$_{oxy}$/NOHA trapped in its A$_{1903}$ conformation.

The photoproduct spectra obtained after slow-cool illumination (Figure 2c) are similar to the ones recorded after 10-s illumination (Figure 2b), suggesting that it is not possible to populate additional docking sites to any significant extent. The greatest difference is seen for iNOS$_{oxy}$-CO. Its photoproduct spectrum shows two well separated bands at 2124 and 2134 cm^{-1} rather than the non-separated doublet seen in Figure 2b. We also note that there is an additional shoulder at 2117 cm^{-1} for iNOS$_{oxy}$-CO/NOHA.

CO rebinding in iNOS$_{oxy}$. To obtain more information on the photoproduct states, TDS measurements were started at 4 K immediately after illumination. Figure 3 displays the contour maps obtained after 10-s illumination at 4 K, with the absorption changes in the A bands and the photoproduct bands in the left and right columns, respectively.

All iNOS$_{oxy}$-CO samples display single-step CO rebinding. This observation indicates that there is only a single kinetic state of the photolyzed protein-ligand complex, and the presence of sharp photoproduct bands indicates that the photolyzed ligands are trapped in transient docking sites with well-defined orientations. In substrate-free iNOS$_{oxy}$-CO, recombination is already maximal at 4 K and extends to ~70 K (Figure 3a, b). Rebinding in the dominant A$_{1951}$ substate of iNOS$_{oxy}$-CO/H4B peaks at 20 K; as in iNOS$_{oxy}$-CO, the process extends to 70 K. Only the minor A$_{1924}$ subpopulation shows a focused rebinding peak at ~60 K (Figure 3c). The photoproduct map does not yield additional information (Figure 3d). Binding of either L-Arg or NOHA in the active site shifts CO rebinding to higher temperatures, suggesting that the hydrogen bonding interaction stabilizes the ligands at the transient docking site against rebinding (Figures 3e and 3g). Maximal rebinding in iNOS$_{oxy}$/NOHA, *i.e.,* in A$_{1903}$ and A$_{1937}$, occurs at 50 – 60 K (Figure 3g). The corresponding photoproduct bands are centered on 2122 and 2133 cm^{-1} (Figure 3h). The contours at 1950 – 1960 cm^{-1} (Figure 3g) represent rebinding in the NOHA-free A$_{1956}$ substate. With L-Arg anchored in the active site, CO ligands return to the heme iron also at ~50 –60 K (Figure 3e). The corresponding photoproduct map shows a concomitant loss of the photoproduct bands at 2150, 2144, 2131 and 2120 cm^{-1}, associating these bands with CO molecules trapped in the vicinity of the substrate (Figure 3f). A population transfer between photoproduct states due to CO rotation[32,51,52] is apparent from the mirror-imaged dashed and solid contours at 2131 and 2144 cm^{-1} at 12 K.

The TDS maps after slow-cool illumination (Figure 4) show only marginal differences to the ones obtained after brief 4-K illumination

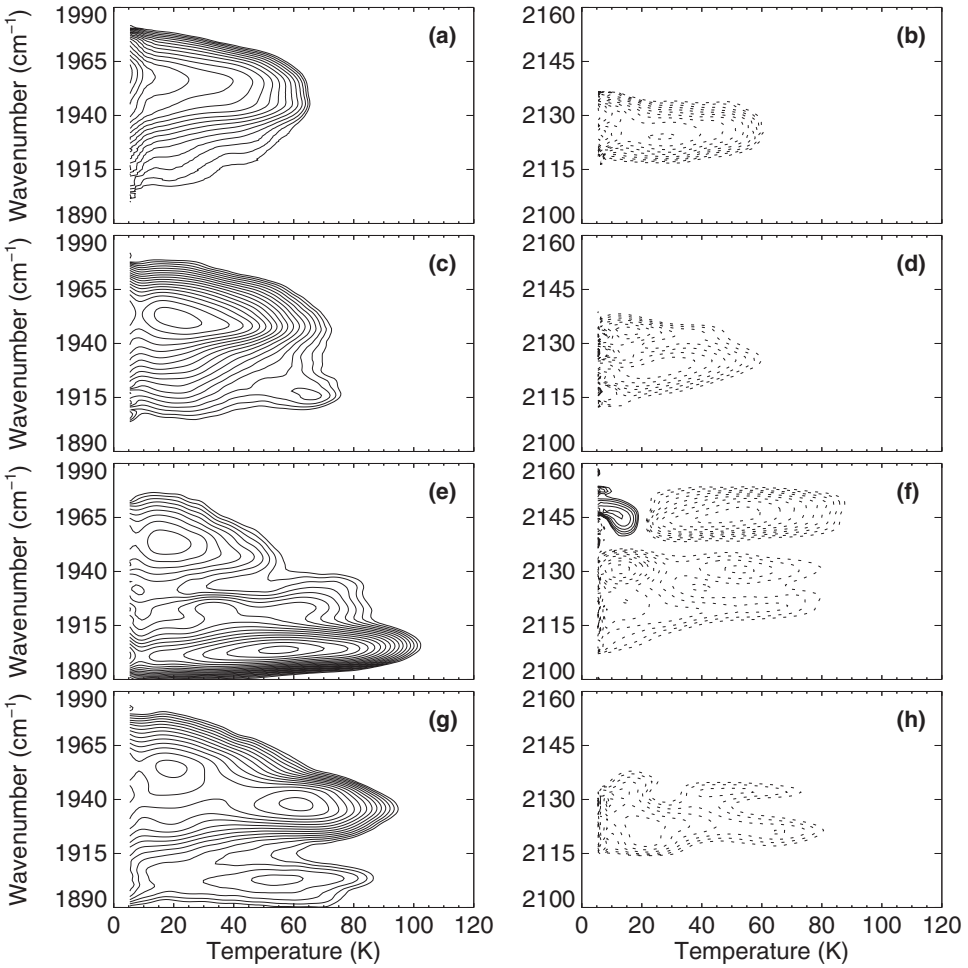

Figure 3. TDS contour maps of iNOS$_{oxy}$-CO, obtained after 10-s illumination at 4 K. Left column: Absorption changes in the bands of heme-bound CO. Right column: Absorption changes in the photoproduct bands. Contours are spaced logarithmically; solid and dotted lines represent increasing and decreasing absorption, respectively. iNOS$_{oxy}$-CO (**a**, **b**) w/o substrate; (**c**, **d**) with H4B; (**d**, **e**) with L-Arg; (**f**, **g**) with NOHA.

(Figure 3), which confirms that the photodissociated CO ligands populate only a single kinetic state. Notably, after slow-cool illumination, rebinding generally occurs at slightly higher temperatures than after brief 4-K illumination. The observed slowing may be attributed to small structural changes near the active site, causing an increase of the ligand binding barrier. A similar effect was also visible in MbCO upon extended illumination below 40 K[42] as well as in NO- and CO-ligated nitrophorin 4[35].

In a typical globin protein involved in ligand transport or storage, the primary ligand docking site B is indispensable because it ensures efficient ligand binding to and release from the heme iron[53]. Incoming ligands are 'caught' in site B before the actual bond formation process occurs[32,54]. Upon thermal dissociation from the heme iron, ligands can remain unbound in site B for some time, which increases their probability to escape from the protein. Without this site, they would immediately recombine with the heme iron, as is, *e.g.*, observed for NO-transporting nitrophorin[35] and modified cytochrome c[55].

The catalytic reaction of iNOS requires sequential binding of two O_2 molecules and efficient release of the NO product. Therefore, the B site is likely to have dual functionality. On the one hand, it allows efficient O_2 binding to the heme iron. On the other hand, it ensures efficient release of the generated NO. Using CO as a ligand, we have shown that the B site is readily accessible for ligands photodissociated from the heme iron, both in the presence and absence of L-Arg or NOHA. The substrates stabilize the CO ligand at the transient site via hydrogen bonding. This stabilizing effect is also seen for the minor A_{1924} subpopulation of iNOS$_{oxy}$/H4B. Presumably, a small fraction of H4B molecules are positioned such that they can form a direct hydrogen bond.

2. FTIR spectroscopy of iNOS$_{oxy}$ using NO as an internal probe

The NO stretching absorption is also very suitable as a local probe of the active site structure and of ligand movements within a protein[17]. Despite their similar sizes, the ligands may show different dynamics inside the protein[56]. For example, in myoglobin (Mb), a transient docking site on the proximal side of the heme is readily populated by CO but not at all by NO[56]. Such subtle differences could be relevant for the inhibitory effects of NO. Therefore, we have analyzed NO binding in ferric iNOS$_{oxy}$ using FTIR-TDS at cryogenic temperatures.

Photolysis difference spectra at 4 K. Figure 5 displays 4-K photolysis difference spectra of various ferric iNOS$_{oxy}$-NO preparations. Most spectra show an A band at 1870 cm^{-1} associated with NO

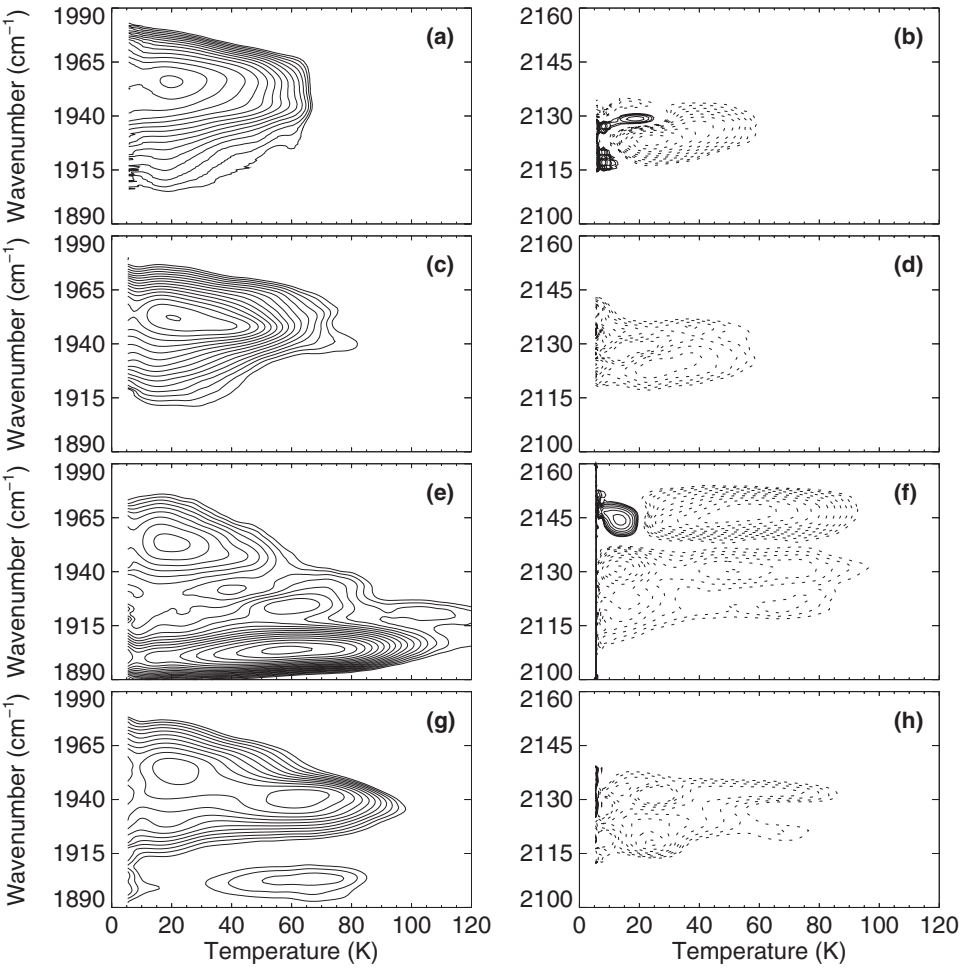

Figure 4. TDS contour maps of iNOS$_{oxy}$-CO, obtained after constant illumination during slow cooling from 160 to 4 K. Left column: Absorption changes in the bands of heme-bound CO. Right column: Absorption changes in the photoproduct bands. Contours are spaced logarithmically; solid and dotted lines represent increasing and decreasing absorption, respectively. iNOS$_{oxy}$-CO (**a**, **b**) w/o substrate; (**c**, **d**) with H4B; (**d**, **e**) with L-Arg; (**f**, **g**) with NOHA.

bound in an active site without bound cofactor or substrate (Table 1). In the spectrum of iNOS$_{oxy}$-NO, A_{1870} is rather broad, suggesting significant conformational heterogeneity at the active site. The spectrum of iNOS$_{oxy}$-NO/NOHA is very similar, dominated by the broad A_{1870} band; the only clear change from iNOS$_{oxy}$-NO is a shoulder at 1851 cm^{-1}. This comparison suggests that NOHA is bound only in a small subfraction reflected by the shoulder. In iNOS$_{oxy}$-NO/L-Arg, A_{1847} and A_{1829} report the binding of L-Arg. A_{1870} is still present due to incomplete saturation with substrate (Figure 5). Interestingly, Rousseau *et al.*[2] could not identify any changes of $\nu_{Fe\text{-}N}$ in their resonance Raman spectra upon binding of L-Arg and even hypothesized that L-Arg does not bind to ferric iNOS$_{oxy}$-NO. With H4B anchored next to the heme, the A band is shifted to 1872 cm^{-1}, and another absorption band emerges at 1890 cm^{-1}.

Most of the observed spectral shifts can again be explained by backbonding[57] because the ferric NO-ligated ground state, which is best described as $Fe^{II}NO^{+}$, is isoelectronic to $Fe^{II}CO$[58]. The heme-bound NO absorbs at 1870 cm^{-1}. L-Arg shifts ν_{NO} to lower frequencies; the A_{1829} and A_{1847} bands indicate an interaction between the NO and the positively charged and neutral terminal amino groups of the L-Arg side chain. As already observed for CO, the effect of NOHA is less pronounced; its presence is visible *via* a shift of the A band to 1851 cm^{-1}. Interestingly, the NO stretching absorption is also affected by H4B. The band shifts slightly and, in addition, it becomes rather narrow, which is indicative of a more homogeneous active site environment or restricted dynamics of the heme-bound NO due to the bound H4B[35,59]. In 2005, Rousseau *et al.*[2] reported that, upon H4B binding, a Raman band emerges that was assigned to the Fe-N-O bending mode, $\delta_{Fe\text{-}N\text{-}O}$, of the ferric adduct, indicating a more homogeneous bending of the bent NO. In thiolate-ligated $Fe^{III}NO$ adducts, NO is typically bound at an angle of 160°[60–66], and H4B binding next to the heme is not expected to modify this angle due to steric interactions. It may, however, restrict its librational dynamics around this angle, possibly because of the increased heme distortion caused by H4B[67,68]. The additional band at 1890 cm^{-1} may indicate partial occupancy of a water molecule in the active site[62].

The photoproduct bands, displayed in Figure 5 with positive amplitudes, are in the 1810 – 1830 cm^{-1} spectral range and, thus, red-shifted

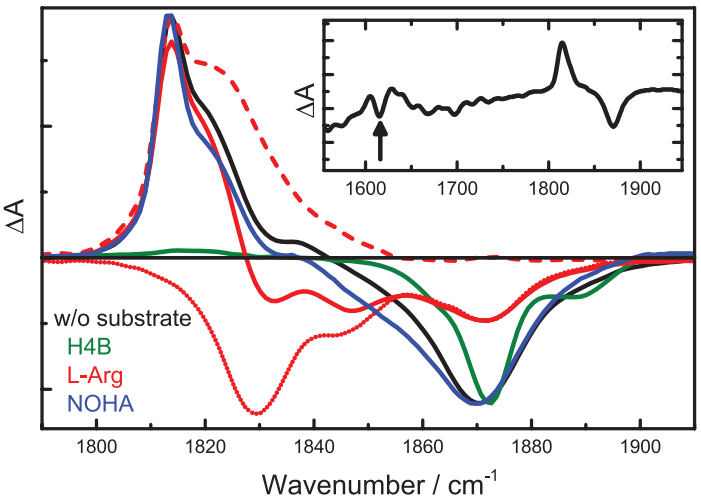

Figure 5. 4-K photolysis difference spectra of iNOS$_{oxy}$-NO. The stretching bands of heme-bound NO (NO after laser illumination at 300 mW) are plotted with negative (positive) amplitude. A bands of the NOHA spectrum were scaled independently of photoproducts (factor 2.07) to match the A bands of the spectrum without substrate. Dotted line: 4-K photolysis difference spectrum of iNOS$_{oxy}$-NO/L-Arg, obtained upon illumination at 0.3 mW. Dashed line: iNOS$_{oxy}$-NO/L-Arg photoproduct spectrum (obtained by calculating the difference between the two iNOS$_{oxy}$-NO/L-Arg spectra). Inset: extended 4-K photolysis difference spectrum of iNOS$_{oxy}$-NO.

by only ~50 cm^{-1} from those of the heme-bound NO (Table 1). For iNOS$_{oxy}$-NO/L-Arg, the photoproduct and A bands even overlap. Their decomposition (details are discussed below) yields a narrow photoproduct band at 1814 cm^{-1} and a broad feature at 1822 cm^{-1}. iNOS$_{oxy}$-NO and iNOS$_{oxy}$-NO/NOHA show two photoproduct bands at 1814 and 1818 cm^{-1}. Interestingly, these bands are about as strong as the A bands, which strongly suggests that they do not represent unbound NO trapped in a transient docking site but rather heme-bound NO with restricted librational freedom.

In contrast to all other samples, the iNOS$_{oxy}$-NO/H4B photoproduct spectrum reveals only a very weak feature at ~1818 cm^{-1}. This finding may be explained by a photolyzed NO that cannot be trapped in well-defined orientations. As a result, the stretching absorption becomes extremely broad and hardly distinguishable from the background. A similar effect was observed for NO in the primary photoproduct site B of ferric Mb[56].

NO rebinding in ferric iNOS$_{oxy}$. To gain additional information on the peculiar, strongly absorbing NO photoproduct bands, TDS experiments were started immediately after illuminating NO-ligated samples at 4 K. Figure 6 displays the absorption changes in the A bands and in the photoproduct bands with solid and dotted lines, respectively. The contour maps obtained after slow cool illumination (not shown) are essentially identical, as for the CO-ligated samples.

In iNOS$_{oxy}$-NO, NO rebinding in A$_{1870}$ starts already at the lowest temperatures (Figure 6a) and extends to ~90 K. The decay of the photoproduct, however, occurs predominantly between 80 and 120 K, indicating that these bands cannot be associated with NO ligands photolyzed from the ferric heme iron, as reported by the A$_{1870}$ band. Apparently, laser illumination produces a photoproduct band from another NO species in the sample. The TDS map of iNOS$_{oxy}$-NO/NOHA (Figure 6d) shows essentially the same features. It is likewise evident that NO rebinding is complete below 80 K, whereas the strange photoproduct feature disappears in the temperature

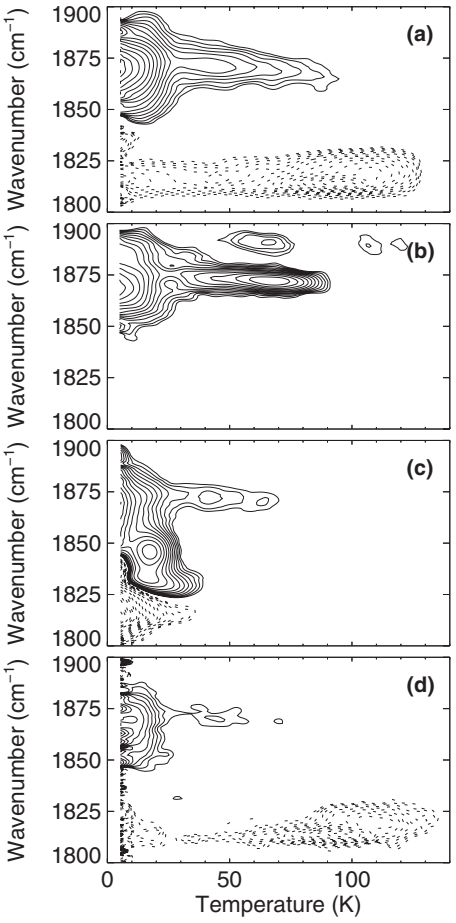

Figure 6. TDS contour maps of iNOS$_{oxy}$-NO, obtained after 30-min illumination at 4 K. iNOS$_{oxy}$-NO (**a**) w/o substrate; (**b**) with H4B; (**c**) with L-Arg; (**d**) with NOHA. Contours are spaced logarithmically; solid and dotted lines represent increasing and decreasing absorption, respectively.

range 80 – 120 K. In $iNOS_{oxy}$-NO/H4B (Figure 6b), NO rebinding at the ferric iron also starts at 4 K. In a subpopulation, recombination peaks at ~65 K; absorption changes of photoproducts are too small to be detected. NO rebinding in the L-Arg-bound A_{1829} and A_{1847} substates occurs mainly below 30 K, concomitantly with the decay of the photoproduct (Figure 6c). The apparent maximum in the contours at 15 K and ~1850 cm^{-1} is artificial and results from the superposition of the A bands and the photoproduct bands (compare Figure 5). Recombination in the substrate-free A_{1870} fraction of the sample is maximal at 4 K and extends out to ~70 K, consistent with the data shown in Figure 6a.

In summary, rebinding of NO to the ferric heme of $iNOS_{oxy}$ is a one-step process. The corresponding photoproduct bands, *i.e.*, the absorption bands of NO photodissociated from the ferric heme, were not identifiable. Presumably, NO is bound only weakly within the protein, without any well-defined orientation and without any additional stabilization via hydrogen bonding interactions to the substrate or the cofactor. As a consequence, the NO has a broad stretching absorption that cannot be distinguished from the background. Note that, if the photoproduct bands were masked by the strong bands at ~1820 cm^{-1}, they should have become visible in the spectrum of $iNOS_{oxy}$-NO/H4B (Figure 5).

Identification of the $iNOS_{oxy}$-NO photoproduct. The TDS data in Figure 5 clearly prove that the strong absorption bands at ~1820 cm^{-1} are not generated by photodissociation of NO bound to ferric heme, absorbing at ~1870 cm^{-1}. To identify the corresponding pre-illumination states, we screened the 4-K FTIR photolysis difference spectrum of $iNOS_{oxy}$-NO from 1,100 to 2,300 cm^{-1} and detected a band at 1616 cm^{-1}, which we tentatively associate with a six-coordinate (6C) ferrous NO adduct (Figure 5, inset). This assignment is supported by the ν_{NO} of 1591 cm^{-1} reported for 6C ferrous $P450_{cam}$-NO[69]. Praneeth *et al.*[70] also computed frequencies in this range, ν_{NO} = 1617 cm^{-1} and ν_{NO} < 1600 cm^{-1} for thiophenolate- and alkylthiolate-heme complexes, respectively, using density functional theory calculations on ferrous, thiolate-coordinated porphyrin model systems.

The admixture of a ferrous NO species in our samples does not come as a surprise. Ferric $iNOS_{oxy}$-NO is unstable and spontaneously converts to a ferrous 6C NO-ligated species. This conversion may take place during loading and cooling of an FTIR sample, which typically takes ~2 h. This species may subsequently evolve further to a five-coordinate (5C) complex by dissociation of the thiolate ligand on time scales of minutes to hours, depending on the $iNOS_{oxy}$ oligomerization state[67,71–73]. Here, we can safely exclude formation of significant amounts of 5C ferrous $iNOS_{oxy}$-NO because we have not observed the characteristic IR bands of this species at ~1670 cm^{-1}[53].

NO photodissociation from the 6C adduct is not expected to generate NO photoproduct bands that are of similar strength as the original A_{1616} band. Therefore, there must be yet another species responsible for the strong absorption at ~1820 cm^{-1}. Perhaps, light-induced breakage of the iron-sulfur rather than the iron-NO bond could lead to an alternative photoproduct, considering the strong *trans* effect exerted by the NO in 6C ferrous heme NO adducts[66]. Indeed, Ibrahim *et al.*[74] had noticed earlier that laser light passing through solution samples of 6C ferrous model porphyrins adducts during resonance Raman measurements was sufficient to photodissociate the axial thiolate base *trans* to the NO[75]. This effect could be suppressed by lowering the temperature to 77 K and reducing the laser power. Accordingly, we have illuminated the $iNOS_{oxy}$-NO/L-Arg sample at low laser intensity (0.3 mW at 532 nm). This power was still sufficient to photodissociate the NO from the 6C ferric heme adduct (dotted line in Figure 5), photoproduct bands at ~1820 cm^{-1}, however, did not emerge, confirming that the photoproduct was not formed. Therefore, we propose that illumination of 6C ferrous $iNOS_{oxy}$-NO with sufficient laser power leads to rupture of the bond between the iron and the proximal Cys194 thiolate, leaving behind a 5C $iNOS_{oxy}$-NO. Because the NO is still bound to the heme iron, the intensity of the IR bands at ~1820 cm^{-1} is comparable to that of other A bands[25,34]. The NO stretching frequency of the 5C adduct indicates that the ligand is coordinated to a ferric iron, so that the Cys194 sulfur is negatively charged after photodissociation. Similar NO stretching frequencies were reported for an isolated 5C ferric heme nitrosyl complex (ν_{NO} = 1842 cm^{-1} [76]) and for NO-ligated porphyrins with phenyl (ν_{NO} = 1825 cm^{-1}) and pentafluorophenyl (ν_{NO} = 1859 cm^{-1}) substituents on the four *meso* positions[77]. If the laser power is sufficiently high (300 mW), it is even possible to photodissociate the NO from the 5C ferric $iNOS_{oxy}$-NO, leaving behind a four-coordinate, 'naked' heme as a 'secondary photoproduct' (Figure 7a).

L-Arg binding in the active site lowers the yield of ferric 5C $iNOS_{oxy}$-NO upon laser illumination (Figures 7a and c) and favors reformation of the iron-sulfur bond as soon as the laser is switched off (Figures 7b and d). This effect may result from the competition between the NO ligand and the thiolate for σ charge donation to the heme iron; the higher the donation, the stronger the bond to the donor and the weaker the bond to the opposing heme ligand. The σ donor strength of the thiolate is altered by hydrogen bonding interactions to the sulfur atom[66]. Using sulfur K-edge x-ray absorption spectroscopy and density functional theory calculations, Dey *et al.*[78] showed that each hydrogen bond reduces the electron-donating power of the thiolate sulfur. The NO electron donor ability and, therefore, its repulsive *trans* effect can be reduced by interactions that draw electron density away from the NO[79,80], here by the hydrogen bonding interaction with L-Arg, so that the axial iron-sulfur bond is stabilized.

We also note that 6C ferrous $iNOS_{oxy}$-NO is not stable in the presence of H4B but spontaneously oxidizes to the ferric form[46]. Consequently, the yield of the 5C adduct is negligible, as is indicated by the low intensity of the absorption bands (Figure 5).

Ferric 5C $iNOS_{oxy}$-NO. In view of the competition between the NO ligand and the thiolate for σ charge donation to the heme iron, one should expect ν_{NO} of the 5C photoproduct lacking the thiolate ligand to be blue-shifted with respect to ν_{NO} of the 6C adduct because the repulsive *trans* effect of the thiolate has been removed. Experimentally, however, the opposite behavior is observed (Figure 5). To resolve this apparent discrepancy, one has to consider that the 5C ferric form originates from a 6C ferrous species, in which the NO is typically bound at an angle of ~140°. In the corresponding 6C ferric derivatives, the Fe – N – O angle is normally ~160°. At cryogenic temperatures, the dynamics of the protein matrix is completely arrested[39,40].

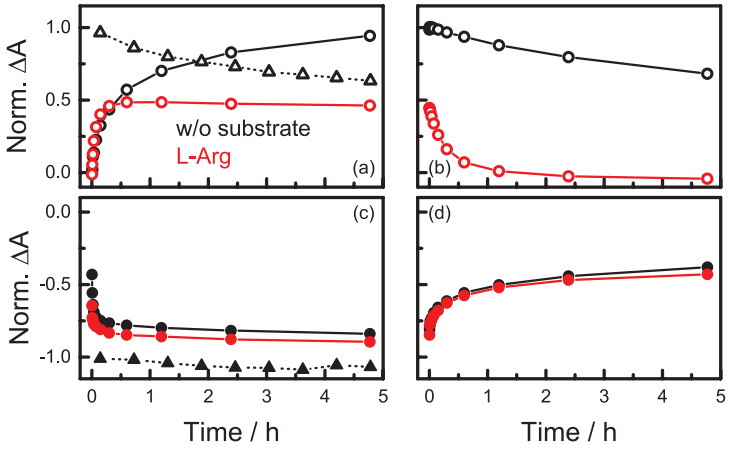

Figure 7. Temporal development of the integrated absorbance of the bands of 5C ferric $iNOS_{oxy}$-NO (open symbols) and 6C ferric $iNOS_{oxy}$-NO (filled symbols) (**a**, **c**) during constant illumination at 4 K (circles: 10 mW, 532 nm; triangles: 300 mW, 532 nm) and (**b**, **d**) after the laser was switched off. Black: $iNOS_{oxy}$-NO; red: $iNOS_{oxy}$-NO/L-Arg.

Consequently, the NO is held in the strongly bent (lower angle) orientation of the 6C ferrous form. Based on DFT calculations, Linder *et al.*[81] reported that reducing the angle from 160° to 150° shifts ν_{NO} in 5C model porphyrins from 1897 to 1857 cm^{-1}. Therefore, we suggest that the low ν_{NO} of the 5C form is caused by NO binding at a small angle. We note that the similar ν_{NO} in 5C and 6C ferric $iNOS_{oxy}$-NO/L-Arg implies that the bound substrate controls the angle at which the NO binds. Apparently, steric constraints override the bending induced by the trans effects.

Finally, we point out that, in contrast to the photo-induced 6C ferric → 5C ferric transition observed in the FTIR experiments at cryogenic temperatures, the spontaneous conversion of the 6C ferric NO-bound $iNOS_{oxy}$ derivative at physiological temperatures involves two NO molecules and yields a 5C ferrous species[71,72,82]. After binding the first NO, the ferric 6C $iNOS_{oxy}$-NO reacts with a second ligand to yield 6C ferrous $iNOS_{oxy}$-NO. This complex immediately converts to the 5C form and a nitrosonium ion (NO^+). The ion may diffuse towards the zinc binding site and nitrosylate one of the Cys residues involved in coordinating the zinc.

Dataset 1. Fourier transform infrared photolysis difference spectra of CO- and NO-ligated inducible nitric oxide synthase

http://dx.doi.org/10.5256/f1000research.5836.d39481

Detailed information on the dataset can be found in the text file "Raw data legend".

Conclusions

FTIR spectroscopy at cryogenic temperatures, especially in combination with sophisticated illumination and data acquisition temperature protocols, provides quantitative data on protein-ligand interactions. Our FTIR-TDS studies on $iNOS_{oxy}$ have shown that CO and NO rebinding involve only a single transient state in $iNOS_{oxy}$. The CO is stabilized in well-defined orientations at the docking site by hydrogen bonding interactions and, therefore, gives rise to rather narrow photoproduct bands. In contrast, photoproduct bands associated with the photolyzed NO cannot be resolved. The NO appears to be trapped in less specific orientations, which may favor the release of this ligand. Under physiological conditions, release of the generated NO from the protein is facilitated.

Upon illumination of 6C ferrous $iNOS_{oxy}$-NO at cryogenic temperatures, a 5C ferric NO adduct was identified, providing direct evidence for light-induced breakage of the iron-thiolate bond. Future studies along these lines are likely to contribute to a better understanding of functional processes in which the NO ligand is involved.

Data availability

F1000Research: Dataset 1. Fourier transform infrared photolysis difference spectra of CO- and NO-ligated inducible nitric oxide synthase, 10.5256/f1000research.5836.d39481[83]

Author contributions

Michael Horn performed the experiments. All authors have contributed to planning the experiments and analyzing the results. All authors were involved in writing and editing the draft of this manuscript. All authors have read and approved the final version.

Competing interests

No competing interests were disclosed.

Grant information

This work was supported by the Deutsche Forschungsgemeinschaft (Grant Ni291/10). We acknowledge support by Deutsche Forschungsgemeinschaft and Open Access Publishing Fund of Karlsruhe Institute of Technology.

The funders had no role in study design, data collection and analysis, decision to publish, or preparation of the manuscript.

References

1. Li HY, Poulos TL: **Structure-function studies on nitric oxide synthases.** *J Inorg Biochem.* 2005; **99**(1): 293–305.
PubMed Abstract | Publisher Full Text
2. Rousseau DL, Li D, Couture M, *et al.*: **Ligand-protein interactions in nitric oxide synthase.** *J Inorg Biochem.* 2005; **99**(1): 306–323.
PubMed Abstract | Publisher Full Text
3. Stuehr DJ: **Mammalian nitric oxide synthases.** *Biochim Biophys Acta.* 1999; **1411**(2–3): 217–230.
PubMed Abstract | Publisher Full Text
4. Crane BR, Arvai AS, Ghosh DK, *et al.*: **Structure of nitric oxide synthase oxygenase dimer with pterin and substrate.** *Science.* 1998; **279**(5359): 2121–2126.
PubMed Abstract | Publisher Full Text
5. Li H, Raman CS, Glaser CB, *et al.*: **Crystal structures of zinc-free and -bound heme domain of human inducible nitric-oxide synthase. Implications for dimer stability and comparison with endothelial nitric-oxide synthase.** *J Biol Chem.* 1999; **274**(30): 21276–21284.
PubMed Abstract | Publisher Full Text
6. Raman CS, Li H, Martasek P, *et al.*: **Crystal structure of nitric oxide synthase heme domains.** *J Inorg Biochem.* 1999; **74**: 44–44.
7. Fischmann TO, Hruza A, Niu XD, *et al.*: **Structural characterization of nitric oxide synthase isoforms reveals striking active-site conservation.** *Nat Struct Biol.* 1999; **6**(3): 233–242.
PubMed Abstract | Publisher Full Text
8. Abu-Soud HM, Yoho LL, Stuehr DJ: **Calmodulin controls neuronal nitric-oxide synthase by a dual mechanism. Activation of intra- and interdomain electron transfer.** *J Biol Chem.* 1994; **269**(51): 32047–32050.
PubMed Abstract
9. Abu-Soud HM, Ichimori K, Nakazawa H, *et al.*: **Regulation of inducible nitric oxide synthase by self-generated NO.** *Biochemistry.* 2001; **40**(2): 6876–6881.
PubMed Abstract | Publisher Full Text
10. Santolini J, Adak S, Curran CM, *et al.*: **A kinetic simulation model that describes catalysis and regulation in nitric-oxide synthase.** *J Biol Chem.* 2001; **276**(2): 1233–1243.
PubMed Abstract | Publisher Full Text
11. Mitchell DA, Erwin PA, Michel T, *et al.*: **S-Nitrosation and regulation of inducible nitric oxide synthase.** *Biochemistry.* 2005; **44**(12): 4636–4647.
PubMed Abstract | Publisher Full Text
12. Smith BC, Fernhoff NB, Marletta MA: **Mechanism and kinetics of inducible nitric oxide synthase auto-S-nitrosation and inactivation.** *Biochemistry.* 2012; **51**(5): 1028–1040.
PubMed Abstract | Publisher Full Text | Free Full Text
13. Rosenfeld RJ, Bonaventura J, Szymczyna BR, *et al.*: **Nitric-oxide synthase forms N-NO-pterin and S-NO-cys: implications for activity, allostery, and regulation.** *J Biol Chem.* 2010; **285**(41): 31581–31589.
PubMed Abstract | Publisher Full Text | Free Full Text
14. Ravi K, Brennan LA, Levic S, *et al.*: **S-nitrosylation of endothelial nitric oxide synthase is associated with monomerization and decreased enzyme activity.** *Proc Natl Acad Sci U S A.* 2004; **101**(8): 2619–2624.
PubMed Abstract | Publisher Full Text | Free Full Text
15. Crane BR, Arvai AS, Gachhui R, *et al.*: **The structure of nitric oxide synthase oxygenase domain and inhibitor complexes.** *Science.* 1997; **278**(5337): 425–431.
PubMed Abstract | Publisher Full Text
16. Garcin ED, Arvai AS, Rosenfeld RJ, *et al.*: **Anchored plasticity opens doors for selective inhibitor design in nitric oxide synthase.** *Nat Chem Biol.* 2008; **4**(11): 700–707.
PubMed Abstract | Publisher Full Text | Free Full Text
17. Nienhaus K, Nienhaus GU: **Ligand dynamics in heme proteins observed by Fourier transform infrared spectroscopy at cryogenic temperatures.** *Methods Enzymol.* 2008; **437**: 347–378.
PubMed Abstract | Publisher Full Text
18. Nienhaus K, Nienhaus GU: **Ligand dynamics in heme proteins observed by Fourier transform infrared-temperature derivative spectroscopy.** *Biochim Biophys Acta.* 2011; **1814**(8): 1030–1041.
PubMed Abstract | Publisher Full Text
19. Vogel KM, Kozlowski PM, Zgierski MZ, *et al.*: **Determinants of the FeXO (X = C, N, O) vibrational frequencies in heme adducts from experiment and density functional theory.** *J Am Chem Soc.* 1999; **121**(43): 9915–9921.
Publisher Full Text
20. Li T, Quillin ML, Phillips GN Jr, *et al.*: **Structural determinants of the stretching frequency of CO bound to myoglobin.** *Biochemistry.* 1994; **33**(6): 1433–1446.
PubMed Abstract | Publisher Full Text
21. Ray GB, Li XY, Ibers JA, *et al.*: **How far can proteins bend the FeCO unit? Distal polar and steric effects in heme proteins and models.** *J Am Chem Soc.* 1994; **116**(1): 162–176.
Publisher Full Text
22. Spiro TG, Ibrahim M, Wasbotten IH: **Chapter 4 - CO, NO, and O2 as Vibrational Probes of Heme Protein Active Sites**. in *The Smallest Biomolecules: Diatomics and their Interactions with Heme Proteins* (Ghosh, A. ed.), Elsevier, Amsterdam. 2008; pp 95–123.
Publisher Full Text
23. Ewing GE: **Infrared Spectra of Liquid and Solid Carbon Monoxide.** *J Chem Phys.* 1962; **37**(10): 2250.
Publisher Full Text
24. Franzen S, Wallace-Williams SE, Shreve AP: **Heme charge-transfer band III is vibronically coupled to the Soret band.** *J Am Chem Soc.* 2002; **124**(24): 7146–7155.
PubMed Abstract | Publisher Full Text
25. Kriegl JM, Nienhaus K, Deng P, *et al.*: **Ligand dynamics in a protein internal cavity.** *Proc Natl Acad Sci U S A.* 2003; **100**(12): 7069–7074.
PubMed Abstract | Publisher Full Text | Free Full Text
26. Park ES, Andrews SS, Hu RB, *et al.*: **Vibrational stark spectroscopy in proteins: A probe and calibration for electrostatic fields.** *J Phys Chem B.* 1999; **103**(45): 9813–9817.
Publisher Full Text
27. Park ES, Boxer SG: **Origins of the sensitivity of molecular vibrations on electric fields: Carbonyl and Nitrosyl Stretches in Model Compounds and Proteins.** *J Phys Chem.* 2002; **106**(22): 5800–5806.
Publisher Full Text
28. Park ES, Thomas MR, Boxer SG: **Vibrational Stark Spectroscopy of NO bound to Heme: Effects of Protein Electrostatic fields on the NO Stretch Frequency.** *J Am Chem Soc.* 2000; **122**(49): 12297–12303.
Publisher Full Text
29. Nienhaus K, Olson JS, Franzen S, *et al.*: **The origin of stark splitting in the initial photoproduct state of MbCO.** *J Am Chem Soc.* 2005; **127**(1): 40–41.
PubMed Abstract | Publisher Full Text
30. Kushkuley B, Stavrov SS: **Theoretical study of the distal-side steric and electrostatic effects on the vibrational characteristics of the FeCO unit of the carbonylheme proteins and their models.** *Biophys J.* 1996; **70**(3): 1214–1229.
PubMed Abstract | Publisher Full Text | Free Full Text
31. Nutt DR, Meuwly M: **Theoretical investigation of infrared spectra and pocket dynamics of photodissociated carbonmonoxy myoglobin.** *Biophys J.* 2003; **85**(6): 3612–3623.
PubMed Abstract | Publisher Full Text | Free Full Text
32. Nienhaus K, Deng P, Kriegl JM, *et al.*: **Structural dynamics of myoglobin: effect of internal cavities on ligand migration and binding.** *Biochemistry.* 2003; **42**(32): 9647–9658.
PubMed Abstract | Publisher Full Text
33. Nienhaus K, Deng P, Kriegl JM, *et al.*: **Structural dynamics of myoglobin: spectroscopic and structural characterization of ligand docking sites in myoglobin mutant L29W.** *Biochemistry.* 2003; **42**(32): 9633–9646.
PubMed Abstract | Publisher Full Text
34. Lehle H, Kriegl JM, Nienhaus K, *et al.*: **Probing electric fields in protein cavities by using the vibrational stark effect of carbon monoxide.** *Biophys J.* 2005; **88**(3): 1978–1990.
PubMed Abstract | Publisher Full Text | Free Full Text
35. Nienhaus K, Maes EM, Weichsel A, *et al.*: **Structural dynamics controls nitric oxide affinity in nitrophorin 4.** *J Biol Chem.* 2004; **279**(38): 39401–39407.
PubMed Abstract | Publisher Full Text
36. Lim M, Jackson TA, Anfinrud PA: **Ultrafast rotation and trapping of carbon monoxide dissociated from myoglobin.** *Nat Struct Biol.* 1997; **4**(3): 209–214.
PubMed Abstract | Publisher Full Text
37. Bredenbeck J, Helbing J, Nienhaus K, *et al.*: **Protein ligand migration mapped by nonequilibrium 2D-IR exchange spectroscopy.** *Proc Natl Acad Sci U S A.* 2007; **104**(36): 14243–14248.
PubMed Abstract | Publisher Full Text | Free Full Text
38. Nienhaus K, Knapp JE, Palladino P, *et al.*: **Ligand migration and binding in the dimeric hemoglobin of Scapharca inaequivalvis.** *Biochemistry.* 2007; **46**(49): 14018–14031.
PubMed Abstract | Publisher Full Text | Free Full Text
39. Nienhaus GU, Heinzl J, Huenges E, *et al.*: **Protein Crystal Dynamics Studied by Time-resolved Analysis of X-ray Diffuse Scattering.** *Nature.* 1989; **338**: 665–666.
Publisher Full Text
40. Frauenfelder H, Nienhaus GU, Johnson JB: **Rate Processes in Proteins.** *Ber Bunsenges Phys Chem.* 1991; **95**(3): 272–278.
Publisher Full Text
41. Berendzen J, Braunstein D: **Temperature-derivative spectroscopy: a tool for protein dynamics.** *Proc Natl Acad Sci U S A.* 1990; **87**(1): 1–5.
PubMed Abstract | Publisher Full Text | Free Full Text
42. Nienhaus GU, Mourant JR, Chu K, *et al.*: **Ligand binding to heme proteins: the effect of light on ligand binding in myoglobin.** *Biochemistry.* 1994; **33**(45): 13413–13430.
PubMed Abstract | Publisher Full Text
43. Mourant JR, Braunstein DP, Chu K, *et al.*: **Ligand binding to heme proteins: II. Transitions in the heme pocket of myoglobin.** *Biophys J.* 1993; **65**(4): 1496–1507.
PubMed Abstract | Publisher Full Text | Free Full Text
44. Ghosh DK, Wu C, Pitters E, *et al.*: **Characterization of the inducible nitric oxide synthase oxygenase domain identifies a 49 amino acid segment required for subunit dimerization and tetrahydrobiopterin interaction.** *Biochemistry.* 1997; **36**(35): 10609–10619.
PubMed Abstract | Publisher Full Text

45. Jung C, Stuehr DJ, Ghosh DK: **FT-Infrared spectroscopic studies of the iron ligand CO stretch mode of iNOS oxygenase domain: effect of arginine and tetrahydrobiopterin.** *Biochemistry.* 2000; **39**(33): 10163–10171.
PubMed Abstract | Publisher Full Text

46. Li D, Stuehr DJ, Yeh SR, *et al.*: **Heme distortion modulated by ligand-protein interactions in inducible nitric-oxide synthase.** *J Biol Chem.* 2004; **279**(25): 26489–26499.
PubMed Abstract | Publisher Full Text

47. Crane BR, Arvai AS, Ghosh S, *et al.*: **Structures of the N(omega)-hydroxy-L-arginine complex of inducible nitric oxide synthase oxygenase dimer with active and inactive pterins.** *Biochemistry.* 2000; **39**(16): 4608–4621.
PubMed Abstract | Publisher Full Text

48. Fukuto JM: **Chemistry of N-hydroxy-L-arginine.** *Methods Enzymol.* 1996; **268**: 365–375.
PubMed Abstract | Publisher Full Text

49. Tantillo DJ, Fukuto JM, Hoffman BM, *et al.*: **Theoretical studies on N-γ-hydroxy-L-arginine and derived radicals: Implications for the mechanism of nitric oxide synthase.** *J Am Chem Soc.* 2000; **122**(3): 536–537.
Publisher Full Text

50. Labby KJ, Li HY, Roman LJ, *et al.*: **Methylated N-ω-Hydroxy-L-arginine Analogues as Mechanistic Probes for the Second Step of the Nitric Oxide Synthase-Catalyzed Reaction.** *Biochemistry.* 2013; **52**(18): 3062–3073.
PubMed Abstract | Publisher Full Text | Free Full Text

51. Lamb DC, Nienhaus K, Arcovito A, *et al.*: **Structural dynamics of myoglobin: ligand migration among protein cavities studied by Fourier transform infrared/temperature derivative spectroscopy.** *J Biol Chem.* 2002; **277**(14): 11636–11644.
PubMed Abstract | Publisher Full Text

52. Nienhaus K, Lamb DC, Deng P, *et al.*: **The effect of ligand dynamics on heme electronic transition band III in myoglobin.** *Biophys J.* 2002; **82**(2): 1059–1067.
PubMed Abstract | Publisher Full Text | Free Full Text

53. Scott EE, Gibson QH, Olson JS: **Mapping the pathways for O_2 entry into and exit from myoglobin.** *J Biol Chem.* **276**(7): 5177–5188.
PubMed Abstract | Publisher Full Text

54. Nienhaus K, Deng P, Olson JS, *et al.*: **Structural dynamics of myoglobin: ligand migration and binding in valine 68 mutants.** *J Biol Chem.* 2003; **278**(43): 42532–42544.
PubMed Abstract | Publisher Full Text

55. Nienhaus K, Zosel F, Nienhaus GU: **Ligand binding to heme proteins: a comparison of cytochrome c variants with globins.** *J Phys Chem B.* 2012; **116**(40): 12180–12188.
PubMed Abstract | Publisher Full Text

56. Nienhaus K, Palladino P, Nienhaus GU: **Structural dynamics of myoglobin: FTIR-TDS study of NO migration and binding.** *Biochemistry.* 2008; **47**(3): 935–948.
PubMed Abstract | Publisher Full Text

57. Soldatova AV, Ibrahim M, Olson JS, *et al.*: **New light on NO bonding in Fe(III) heme proteins from resonance Raman spectroscopy and DFT modeling.** *J Am Chem Soc.* **132**(13): 4614–4625.
PubMed Abstract | Publisher Full Text | Free Full Text

58. Praneeth VK, Paulat F, Berto TC, *et al.*: **Electronic structure of six-coordinate iron(III)-porphyrin NO adducts: the elusive iron(III)-NO(radical) state and its influence on the properties of these complexes.** *J Am Chem Soc.* 2008; **130**(46): 15288–15303.
PubMed Abstract | Publisher Full Text

59. Batabyal D, Yeh SR: **Human tryptophan dioxygenase: a comparison to indoleamine 2,3–dioxygenase.** *J Am Chem Soc.* 2007; **129**(50): 15690–15701.
PubMed Abstract | Publisher Full Text

60. Xu N, Powell DR, Cheng L, *et al.*: **The first structurally characterized nitrosyl heme thiolate model complex.** *Chem Commun (Camb).* 2006; (19): 2030–2032.
PubMed Abstract | Publisher Full Text

61. Obayashi E, Tsukamoto K, Adachi S, *et al.*: **Unique binding of nitric oxide to ferric nitric oxide reductase from *Fusarium oxysporum* elucidated with infrared, resonance Raman, and X-ray absorption spectroscopies.** *J Am Chem Soc.* 1997; **119**: 7807–7816.
Publisher Full Text

62. Li H, Igarashi J, Jamal J, *et al.*: **Structural studies of constitutive nitric oxide synthases with diatomic ligands bound.** *J Biol Inorg Chem.* 2006; **11**(6): 753–768.
PubMed Abstract | Publisher Full Text

63. McQuarters AB, Wirgau NE, Lehnert N: **Model complexes of key intermediates in fungal cytochrome P450 nitric oxide reductase (P450nor).** *Curr Opin Chem Biol.* 2014; **19**: 82–89.
PubMed Abstract | Publisher Full Text

64. Shimizu H, Obayashi E, Gomi Y, *et al.*: **Proton delivery in NO reduction by fungal nitric-oxide reductase. Cryogenic crystallography, spectroscopy, and kinetics of ferric-NO complexes of wild-type and mutant enzymes.** *J Biol Chem.* 2000; **275**(7): 4816–4826.
PubMed Abstract | Publisher Full Text

65. Pant K, Crane BR: **Nitrosyl-heme structures of *Bacillus subtilis* nitric oxide synthase have implications for understanding substrate oxidation.** *Biochemistry.* 2006; **45**(8): 2537–2544.
PubMed Abstract | Publisher Full Text

66. Goodrich LE, Paulat F, Praneeth VK, *et al.*: **Electronic structure of heme-nitrosyls and its significance for nitric oxide reactivity, sensing, transport, and toxicity in biological systems.** *Inorg Chem.* 2010; **49**(14): 6293–6316.
PubMed Abstract | Publisher Full Text

67. Couture M, Adak S, Stuehr DJ, *et al.*: **Regulation of the properties of the heme-NO complexes in nitric-oxide synthase by hydrogen bonding to the proximal cysteine.** *J Biol Chem.* 2001; **276**(41): 38280–38288.
PubMed Abstract | Publisher Full Text

68. Rousseau DL, Li D, Hayden EY, *et al.*: **Chapter 17 - Ligand-Protein Interactions in Mammalian Nitric Oxide Synthase**. in *The Smallest Biomolecules: Diatomics and their Interactions with Heme Proteins* (Ghosh, A. ed.), Elsevier, Amsterdam. 2008; pp 465–497.
Publisher Full Text

69. Hu SZ, Kincaid JR: **Resonance Raman Spectra of the Nitric Oxide Adducts of Ferrous Cytochrome P450cam in the Presence of Various Substrates.** *J Am Chem Soc.* 1991; **113**(26): 9760–9766.
Publisher Full Text

70. Praneeth VK, Haupt E, Lehnert N: **Thiolate coordination to Fe(II)-porphyrin NO centers.** *J Inorg Biochem.* 2005; **99**(4): 940–948.
PubMed Abstract | Publisher Full Text

71. Li D, Hayden EY, Panda K, *et al.*: **Regulation of the monomer-dimer equilibrium in inducible nitric-oxide synthase by nitric oxide.** *J Biol Chem.* 2006; **281**(12): 8197–8204.
PubMed Abstract | Publisher Full Text

72. Abu-Soud HM, Wu C, Ghosh DK, *et al.*: **Stopped-flow analysis of CO and NO binding to inducible nitric oxide synthase.** *Biochemistry.* 1998; **37**(11): 3777–3786.
PubMed Abstract | Publisher Full Text

73. Wang J, Rousseau DL, Abu-Soud HM, *et al.*: **Heme coordination of NO in NO synthase.** *Proc Natl Acad Sci U S A.* 1994; **91**(22): 10512–10516.
PubMed Abstract | Publisher Full Text | Free Full Text

74. Ibrahim M, Xu CL, Spiro TG: **Differential sensing of protein influences by NO and CO vibrations in heme adducts.** *J Am Chem Soc.* 2006; **128**(51): 16834–16845.
PubMed Abstract | Publisher Full Text | Free Full Text

75. Coyle CM, Vogel KM, Rush TS 3rd, *et al.*: **FeNO structure in distal pocket mutants of myoglobin based on resonance Raman spectroscopy.** *Biochemistry.* 2003; **42**(17): 4896–4903.
PubMed Abstract | Publisher Full Text

76. Chiavarino B, Crestoni ME, Fornarini S, *et al.*: **Direct probe of NO vibration in the naked ferric heme nitrosyl complex.** *Chemphyschem.* 2008; **9**(6): 826–828.
PubMed Abstract | Publisher Full Text

77. Lanucara F, Chiavarino B, Crestoni ME, *et al.*: **Naked five-coordinate Fe(III)(NO) porphyrin complexes: vibrational and reactivity features.** *Inorg Chem.* 2011; **50**(10): 4445–4452.
PubMed Abstract | Publisher Full Text

78. Dey A, Okamura TA, Ueyama N, *et al.*: **Sulfur K-edge XAS and DFT calculations on P450 model complexes: effects of hydrogen bonding on electronic structure and redox potentials.** *J Am Chem Soc.* 2005; **127**(34): 12046–12053.
PubMed Abstract | Publisher Full Text | Free Full Text

79. Decatur SM, Franzen S, DePillis GD, *et al.*: **Trans effects in nitric oxide binding to myoglobin cavity mutant H93G.** *Biochemistry.* 1996; **35**(15): 4939–4944.
PubMed Abstract | Publisher Full Text

80. Fernandez ML, Marti MA, Crespo A, *et al.*: **Proximal effects in the modulation of nitric oxide synthase reactivity: a QM-MM study.** *J Biol Inorg Chem.* 2005; **10**(6): 595–604.
PubMed Abstract | Publisher Full Text

81. Linder DP, Rodgers KR, Banister J, *et al.*: **Five-coordinate Fe(III)NO and Fe(II)CO porphyrinates: where are the electrons and why does it matter?** *J Am Chem Soc.* 2004; **126**(43): 14136–14148.
PubMed Abstract | Publisher Full Text | Free Full Text

82. Huang L, Abu-Soud HM, Hille R, *et al.*: **Nitric oxide-generated P420 nitric oxide synthase: characterization and roles for tetrahydrobiopterin and substrate in protecting against or reversing the P420 conversion.** *Biochemistry.* 1999; **38**(6): 1912–1920.
PubMed Abstract | Publisher Full Text

83. Horn M, Nienhaus K, Nienhaus GU: **Fourier transform infrared photolysis difference spectra of CO- and NO-ligated inducible nitric oxide synthase.** *F1000Research.* 2014.
Data Source